Figures and figure supplements

Oldest skeleton of a fossil flying squirrel casts new light on the phylogeny of the group

Isaac Casanovas-Vilar *et al*

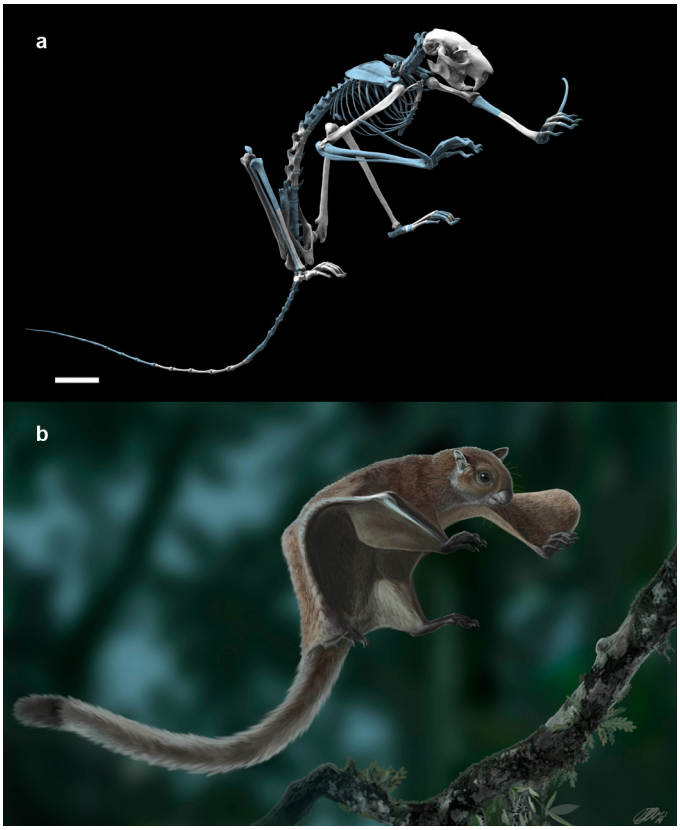

Figure 1. The fossil flying squirrel *Miopetaurista neogrivensis*. (**a**) Reconstruction of the skeleton based in the partial skeleton IPS56468 from Abocador de Can Mata. Missing elements are based on extant giant flying squirrel *Petaurista petaurista* and are colored in blue. (**b**) Life appearance of *Miopetaurista neogrivensis* showing the animal ready to land on a tree branch. Coat pattern and color are based in extant *Petaurista* species, the sister taxon of *Miopetaurista* (see ***Figure 7***). See ***Video 1*** for an animated version of this reconstruction and 3D model in ***Supplementary file 1*** to view and manipulate a low-quality model of the skeleton. For recovered elements of the postcranial skeleton see ***Figures 2*** and ***4*** and ***Table 1***. For a description and comparison of the postcranial bones, see Appendix 3.3. See ***Figure 6*** and ***Video 3*** for a more detailed cranial reconstruction. 3D models generated from µCT scan data and photogrammetry. Scale bar is 4 cm.

DOI: https://doi.org/10.7554/eLife.39270.003

Figure 2. Selected postcranial elements of the partial skeleton of *Miopetaurista neogrivensis*. (**a–b**) Right humerus (IPS56468f) in cranial and caudal views. (**c–d**) Right femur (IPS56468b) in cranial and caudal views. (**e–f**) Right tibia (IPS56468a) in cranial and caudal views. (**g–h**) Lumbar vertebrae L3–L6 (IPS56468m–n) in dorsal and ventral views. Note that vertebrae are in anatomical connection. (**i–j**) Partial right coxal (IPS56468k) in lateral and medial views. The proximal end of the ilium is not preserved and part of the pubis is damaged. (**k–l**) Left astragalus (IPS56478t). (**m–n**) Left calcaneus (IPS56468s). fp, fibular process; st, sulcus tali; sup, sustentacular process. Scale bar is 2 cm in figures (**a–j**) and 1 cm in figures (**k–n**). For a reconstruction of the skeleton see ***Figure 1***, ***Videos 1*** and ***3D*** model in ***Supplementary file 1***. Details of particular bones are shown in ***Figure 5***; ***Figure 2—figure supplement 1***. For a detailed description and comparison of the postcranial bones of *M. neogrivensis* see Appendix 3.3.

DOI: https://doi.org/10.7554/eLife.39270.004

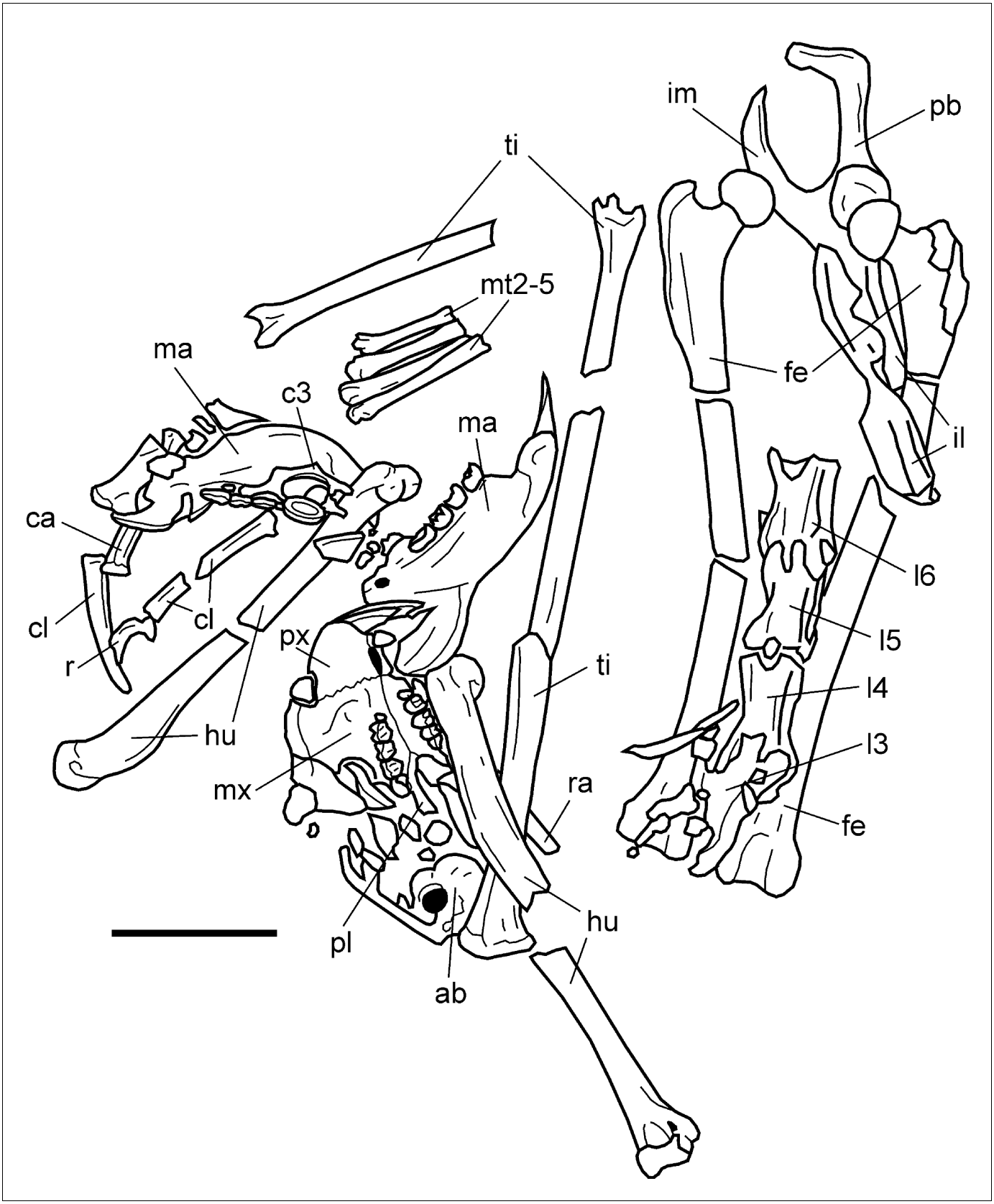

Figure 2—figure supplement 1. Schematic drawing of the recovered skeletal elements of *Miopetaurista neogrivensis* from Abocador de Can Mata locality ACM/C5-D1 (IPS56468) in the position that they were found. Note that some elements, such as the femora, pelvis and tail vertebrae are in

Figure 2—figure supplement 1 continued on next page

Figure 2—figure supplement 1 continued

anatomical connection. This scheme has been drawn based on multiple pictures taken during the preparation process. Not all the elements shown here were visible at the same time, many of them being unearthed during the separation of the specimen from the matrix. ab, auditory bulla; c3, cervical vertebra 3; ca, caudal vertebra; cl, clavicle; fe, femur; hu, humerus; il, ilium; im, ischium, l3–l6, lumbar vertebrae 3 to 6; ma, mandible; mt2–5, metatarsals 2 to 5 in anatomical connection; mx, maxilla; pb, pubis; pl, palatine; px, premaxilla; r, rib; ra, radius; ti, tibia. For a complete catalogue of the recovered elements of the partial skeleton IPS56468 see ***Table 1***. Scale bar is 5 cm.

DOI: https://doi.org/10.7554/eLife.39270.005

Figure 3. Mandible and cheek teeth of *Miopetaurista neogrivensis*. (**a** to **c**) Partial left hemimandible (IPS56468j) in lateral, medial and dorsal views. (**d** to **e**) Partial right hemimandible (IPS56468i) in lateral and medial views. A caudal vertebra and a bone fragment are attached to the lateral side of the mandibular ramus. Both hemimandibles were associated to the partial skeleton IPS56468 from ACM/C5-D1. (**f** to **g**) Partial hemimandible (IPS87560) from ACM/C8-B sector in lateral and medial views. (**h**) Left upper cheek teeth series (P3–M3) of IPS56468h (***Figure 6—Figure supplement 1***). (**i**) Left lower cheek teeth series (p4–m3) of IPS56468j. Cheek teeth measurements are given in ***Supplementary file 4*** whereas mandibular measurements are given in ***Supplementary file 6***. For a detailed description and comparisons of cheek teeth and mandible morphology see Appendix 3.1 and 3.2. an, angular process; ar, articular process; co, coronoid process. Scale bar is 1 cm in figs. a to g; 2 mm in (**h to i**).

DOI: https://doi.org/10.7554/eLife.39270.006

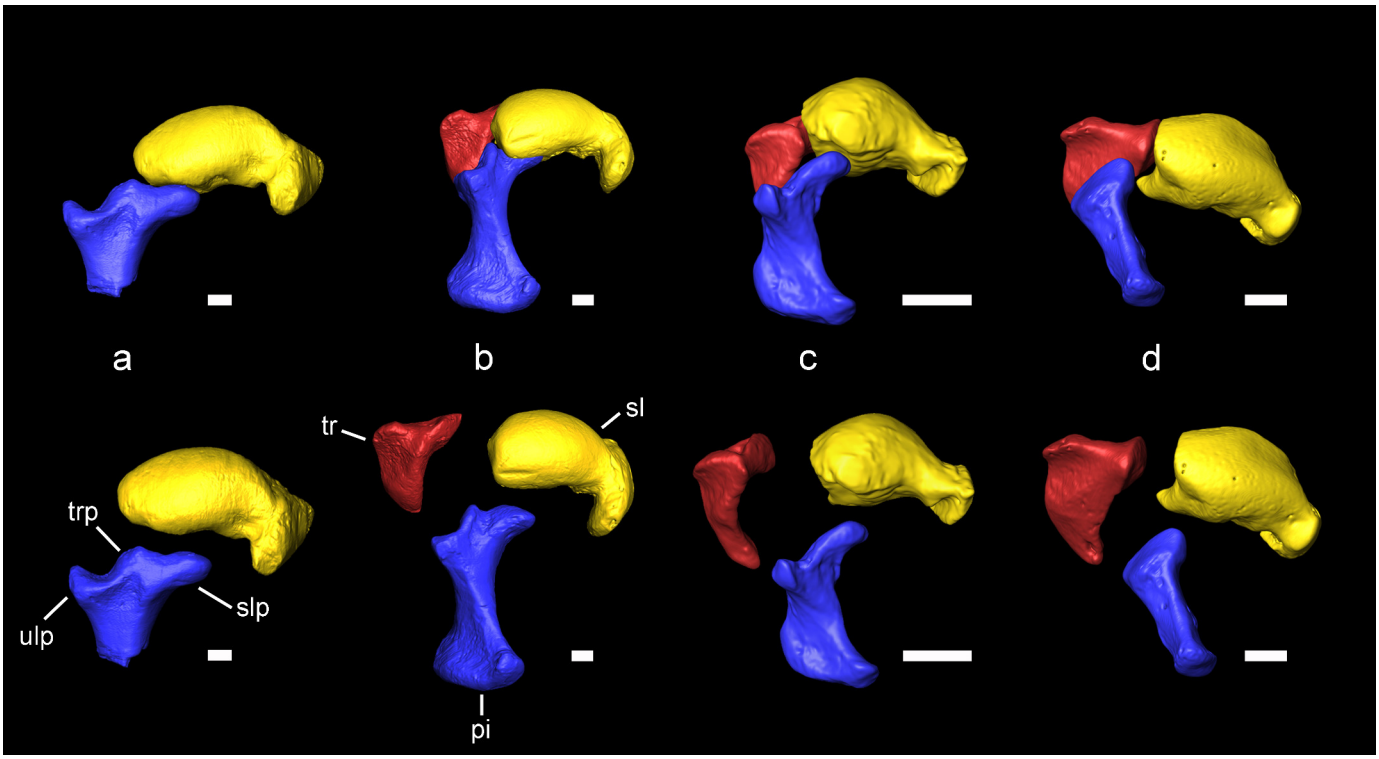

Figure 4. Carpal bones associated with the extension of the patagium of *Miopetaurista neogrivensis* as compared to extant squirrels. Articulated bones are shown on top and disarticulated ones are shown below. (**a**) *Miopetaurista neogrivensis*. (**b**) *Petaurista petaurista*, large-sized flying squirrel, subtribe Pteromyina. (**c**) *Hylopetes sagitta*, small-sized flying squirrel, subtribe Glaucomyina. (**d**) *Sciurus vulgaris*, tree squirrel, tribe Sciurini. The patagium is supported by the styliform cartilage which is attached to the pisiform bone. Flying squirrels present an elevated process for articulation with the scapholunate in the pisiform, whereas in tree squirrels this bone only articulates with the triquetrum and the ulna. In addition, note the presence of a triquetral process in *Miopetaurista* and *Petaurista*, characteristic of the Pteromyina. All extant specimens are kept in the collections of the Naturalis Biodiversity Center (Leiden, the Netherlands). See ***Video 2*** for an animated version of this figure. Collection numbers of the scanned specimens and computed tomography parameters used are given in ***Table 5***. Tridimensional models generated from µCT scan data. pi, pisiform (in blue); sl, scapholunate (in yellow); slp, scapholunate process of the pisiform; tr, triquetrum (in red); trp, triquetral processes of the pisiform; ulp, ulnar process of the pisiform. Scale bar is 1 cm.

DOI: https://doi.org/10.7554/eLife.39270.007

Figure 5. Comparison of the limb bones of extant ground, tree and flying squirrels with *Miopetaurista neogrivensis*. All elements are scaled to femur length and shown in anterior view. Humerus (**a–e**) and articulated femur and tibia (**f–j**) of: (**a,f**) the xerin ground squirrel *Xerus erythropus*; (**b,g**) the

Figure 5 continued on next page

Figure 5 continued

callosciurin tree squirrel *Callosciurus prevostii*; (**c,h**) the small-sized flying squirrel (subtribe Glaucomyina) *Hylopetes sagitta*; (**d,i**) the large-sized fying squirrel (subtribe Pteromyina) *Petaurista petaurista*; (**e,j**) *Miopetaurista neogrivensis*. Note that limb bones of flying squirrels and *M. neogrivensis* are much longer and more slender than those of tree and ground squirrels. Furthermore, processes and areas for the insertion of the main limb muscles are reduced. For a description and comparison of the postcranial bones of *M. neogrivensis*, see Appendix 3.3. See ***Supplementary file 7*** for the collection numbers of the figured specimens and postcranial measurements. All bones are right elements, except for a–b and f–g, which are reversed left elements. Scale bar is 1 cm.

DOI: https://doi.org/10.7554/eLife.39270.008

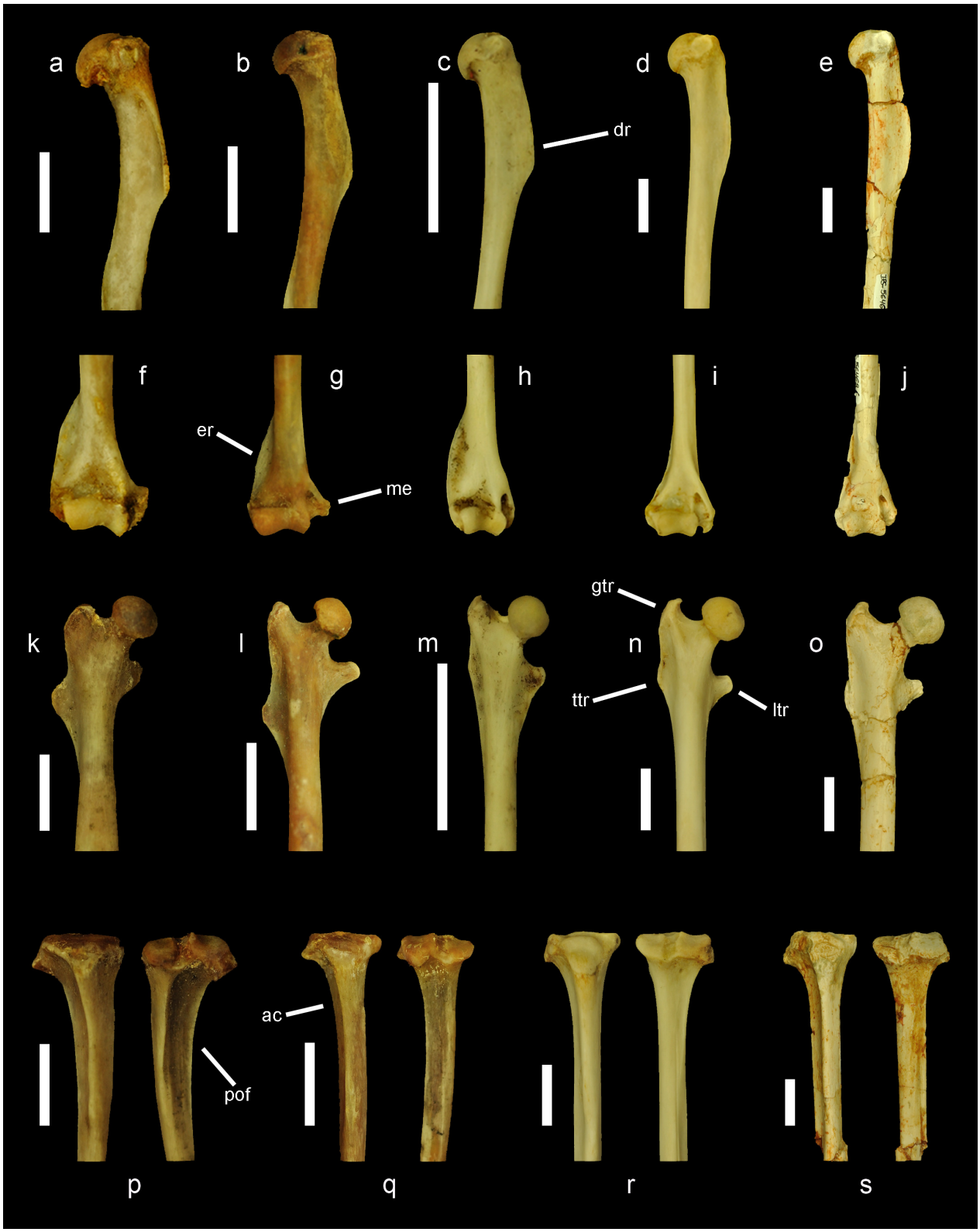

Figure 5—figure supplement 1. Comparison of the proximal and distal ends of the humerus, femur and tibia of extant ground, tree and flying squirrels with *Miopetaurista neogrivensis*. (**a** to **e**) Proximal end of the humerus in lateral view. (**f** to **j**) Distal end of the humerus in anterior view. (**k** to **o**)

Figure 5—figure supplement 1 continued on next page

Figure 5—figure supplement 1 continued

proximal end of the femur in anterior view. (**p** to s) Proximal end of the tibia in anterior (left) and posterior (right) views. Figured specimens belong to: the marmotin ground squirrel *Urocitellus paryii* (**a, f, k, p**); the callosciurin tree squirrel *Callosciurus prevostii* (**b, g, l, q**); the small-sized flying squirrel (subtribe Glaucomyina) *Hylopetes sagitta* (**c, h, m**); the large-sized flying squirrel (subtribe Pteromyina) *Petaurista petaurista* (**d, i, n, r**); and *Miopetaurista neogrivensis* (**e, j, o, s**). All bones are right elements, except for b, g, l and q, which are reversed left elements. ac, anterior crest; dr, deltoid ridge; er, epicondylar ridge; gtr, greater trochanter; ltr, lesser trochanter; me, medial epicondyle; pof, popliteal fossa; ttr, third trochanter. Scale bar is 1 cm.

DOI: https://doi.org/10.7554/eLife.39270.009

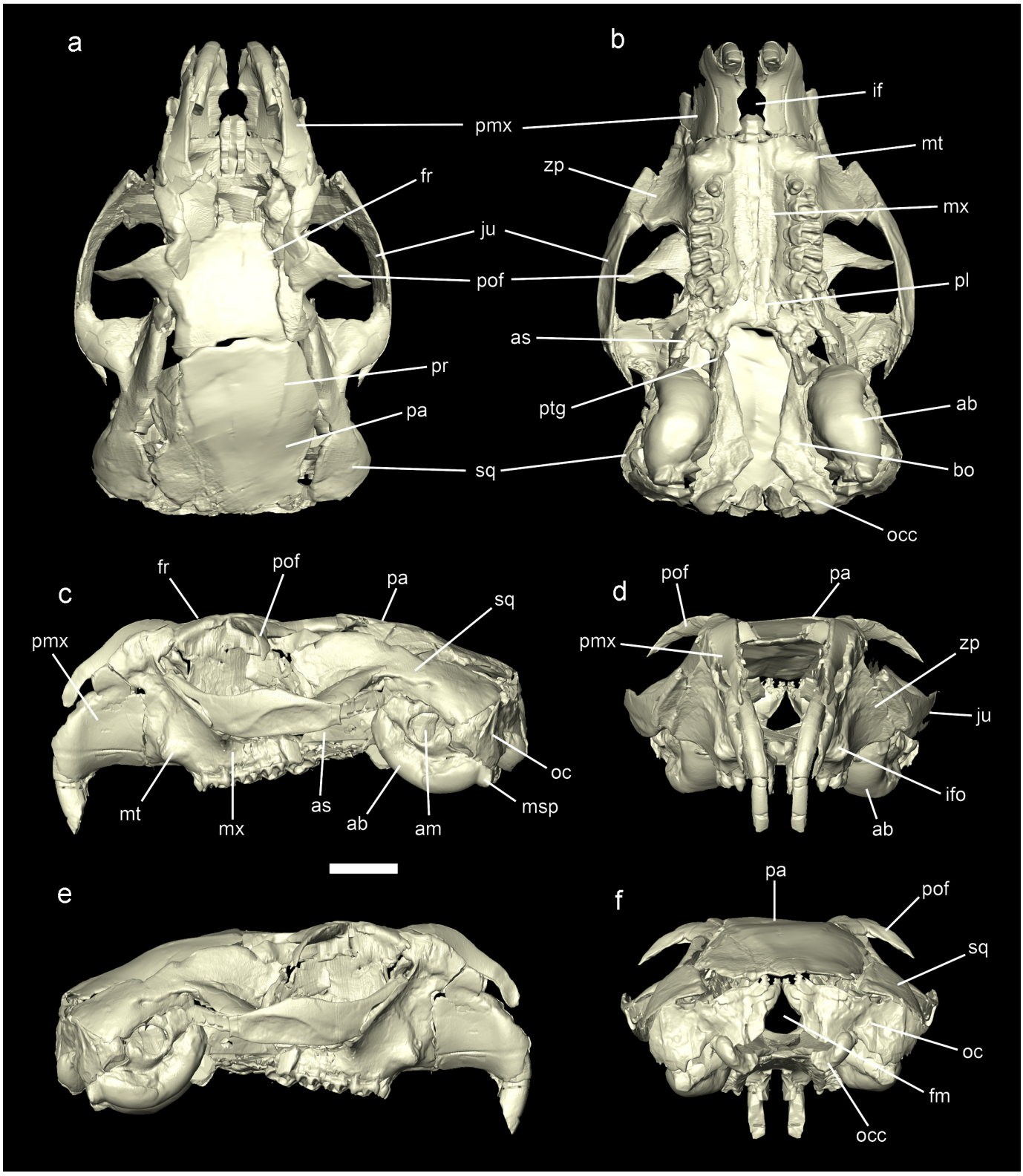

Figure 6. Reconstruction of the cranium of *Miopetaurista neogrivensis*. Virtual reconstruction based on µCT scan data from specimens IPS56468h (see ***Figure 6—figure supplement 1***) and IPS88677 (see ***Figure 6—figure supplement 2***). Specimen IPS56468h was used as the basis for the

Figure 6 continued on next page

Figure 6 continued

reconstruction, with missing elements taken from IPS88677 (***Table 3***. (**a**) Dorsal view. (**b**) Ventral view. (**c**) Lateral (left) view. (**d**) Anterior view. (**e**) Lateral (right) view. (**f**) Posterior view. See ***Video 3*** for an animated version of the skull reconstruction. For a detailed description of skull morphology see Appendix 3.2. Cranial measurements for original fossil specimens (IPS56468h, IPS88677) as well as for the virtually reconstructed cranium are given in ***Supplementary file 5***. ab, auditory bulla; am, auditory meatus; as, alisphenoid; bo, basioccipital; fm, foramen magnum; fr, frontal; if, incisive foramen; ifo, infraorbital foramen; ju, jugal; msp, mastoid process; mt, masseteric tubercle; mx, maxillary; oc, occipital; occ, occipital condyle; pa, parietal; pl, palatine; pmx, premaximallary; pof, postorbital process of the frontal; pr, parietal ridges; ptg, pterygoid; sq, squamosal; zp, zygomatic plate. Scale bar is 1 cm.

DOI: https://doi.org/10.7554/eLife.39270.014

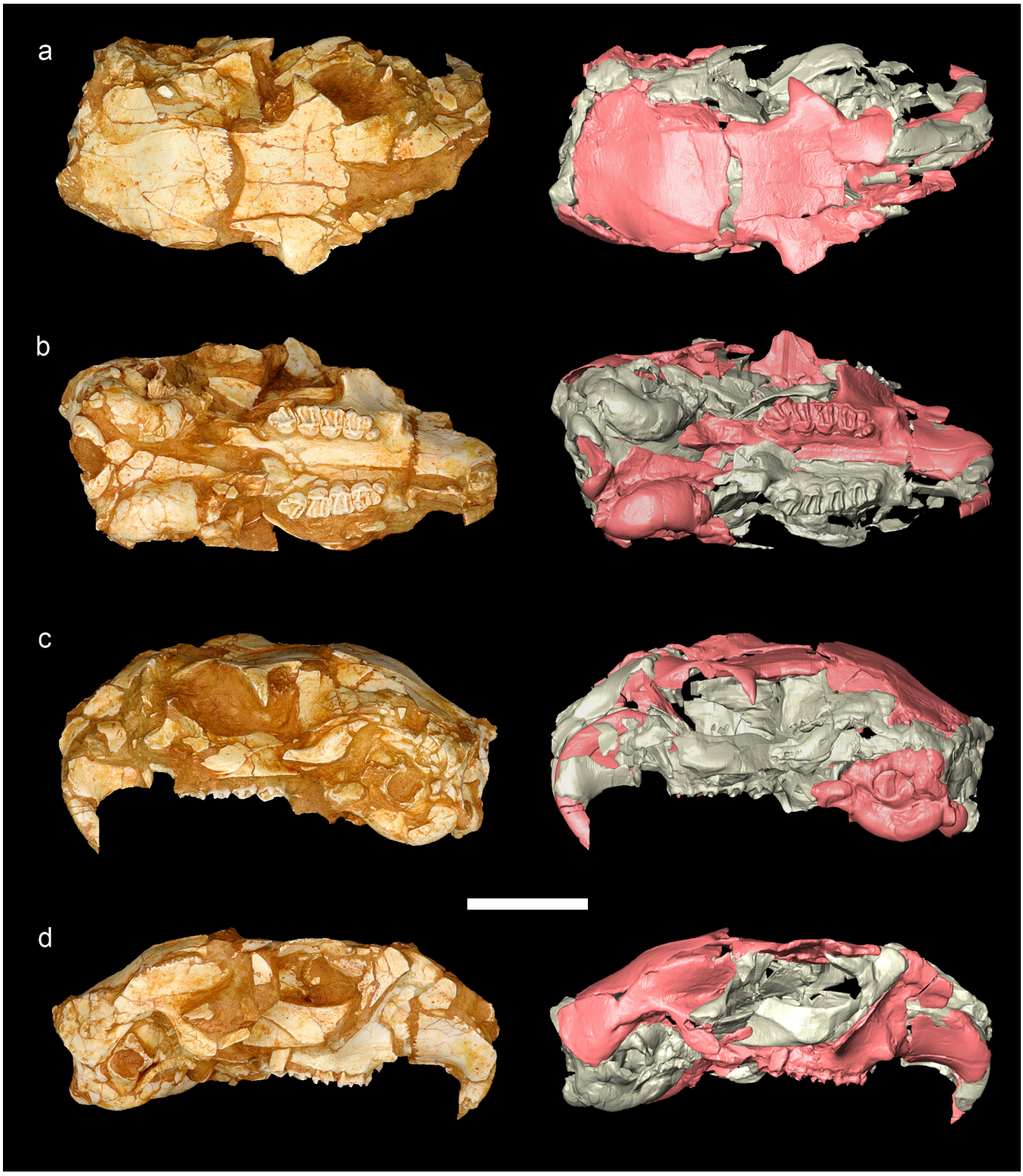

Figure 6—figure supplement 1. Cranium of *Miopetaurista neogrivensis* associated with partial skeleton IPS56468. The partial skull (IPS56468h) belongs to the same individual as the partial skeleton IPS56468 from Abocador de Can Mata locality ACM/C5-D1. Fossil specimens are shown on the left,

Figure 6—figure supplement 1 continued on next page

Figure 6—figure supplement 1 continued

whereas tridimensional models based on µCT scan data are shown on the right. (**a**) Dorsal view. (**b**) Ventral view. (**c**) Lateral (left) view. (**d**) Lateral (right) view. Note that the cranium is obliquely crushed but not plastically deformed. Parts used in the reconstruction of the skull of *M. neogrivensis* are colored in pink. Cranial measurements are given in ***Supplementary file 5***. Scale bar is 1 cm.

DOI: https://doi.org/10.7554/eLife.39270.015

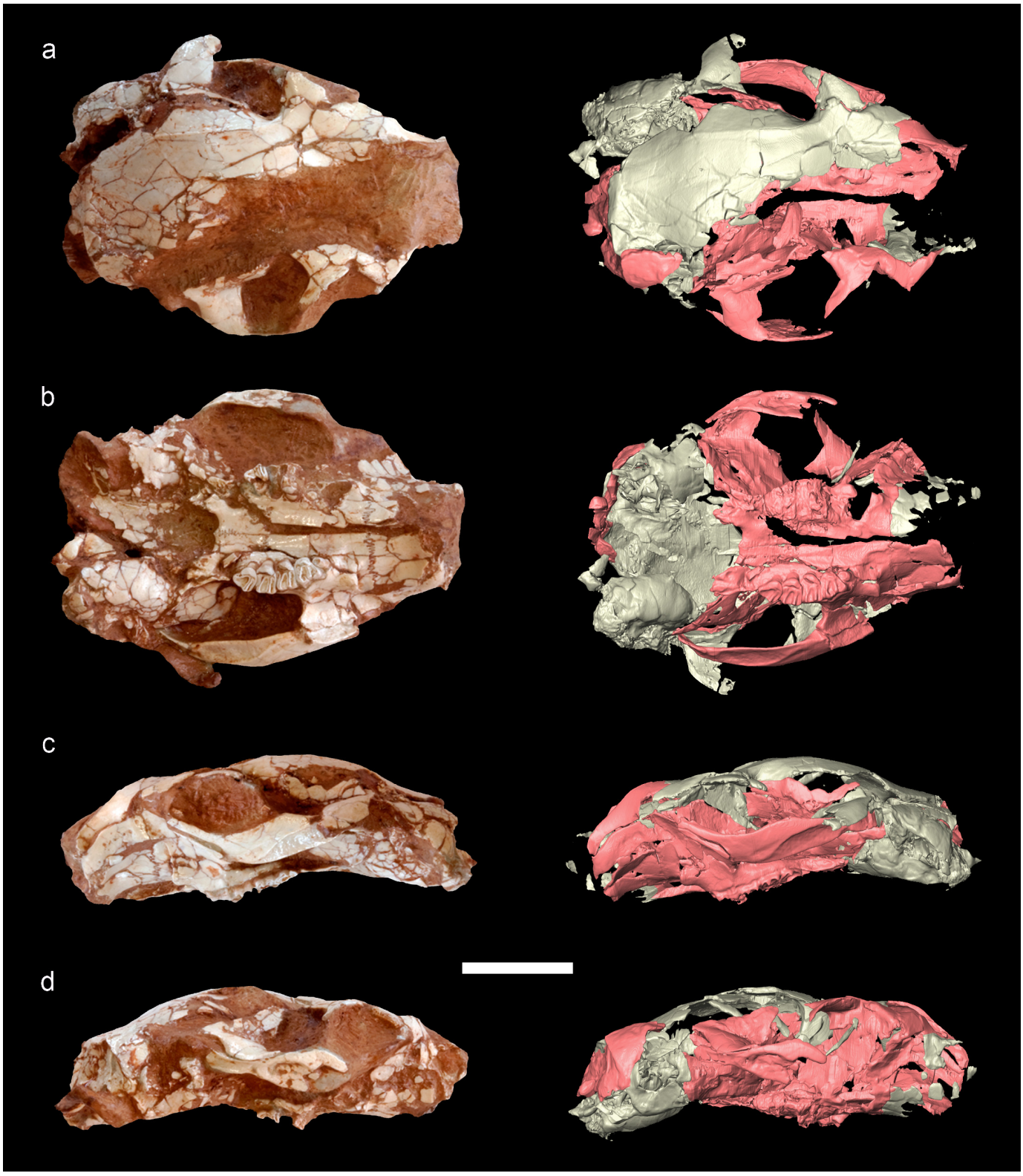

Figure 6—figure supplement 2 Cranium of *Miopetaurista neogrivensis* (IPS88677) from Abocador de Can Mata locality ACM/C8-Af. Fossil specimens are shown on the left, whereas tridimensional models based on µCT scan data are shown on the right. (**a**) Dorsal view. (**b**) Ventral view. (**c**) Lateral (left)

Figure 6—figure supplement 2 continued on next page

Figure 6—figure supplement 2 continued

view. (**d**) Lateral (right) view. Note that the skull is dorsoventrally crushed and most of the premaxillary and frontal bones are not preserved. Parts used in the reconstruction of the skull of *M. neogrivensis* are colored in pink. Cranial measurements are given in ***Supplementary file 5***. Scale bar is 1 cm.

DOI: https://doi.org/10.7554/eLife.39270.016

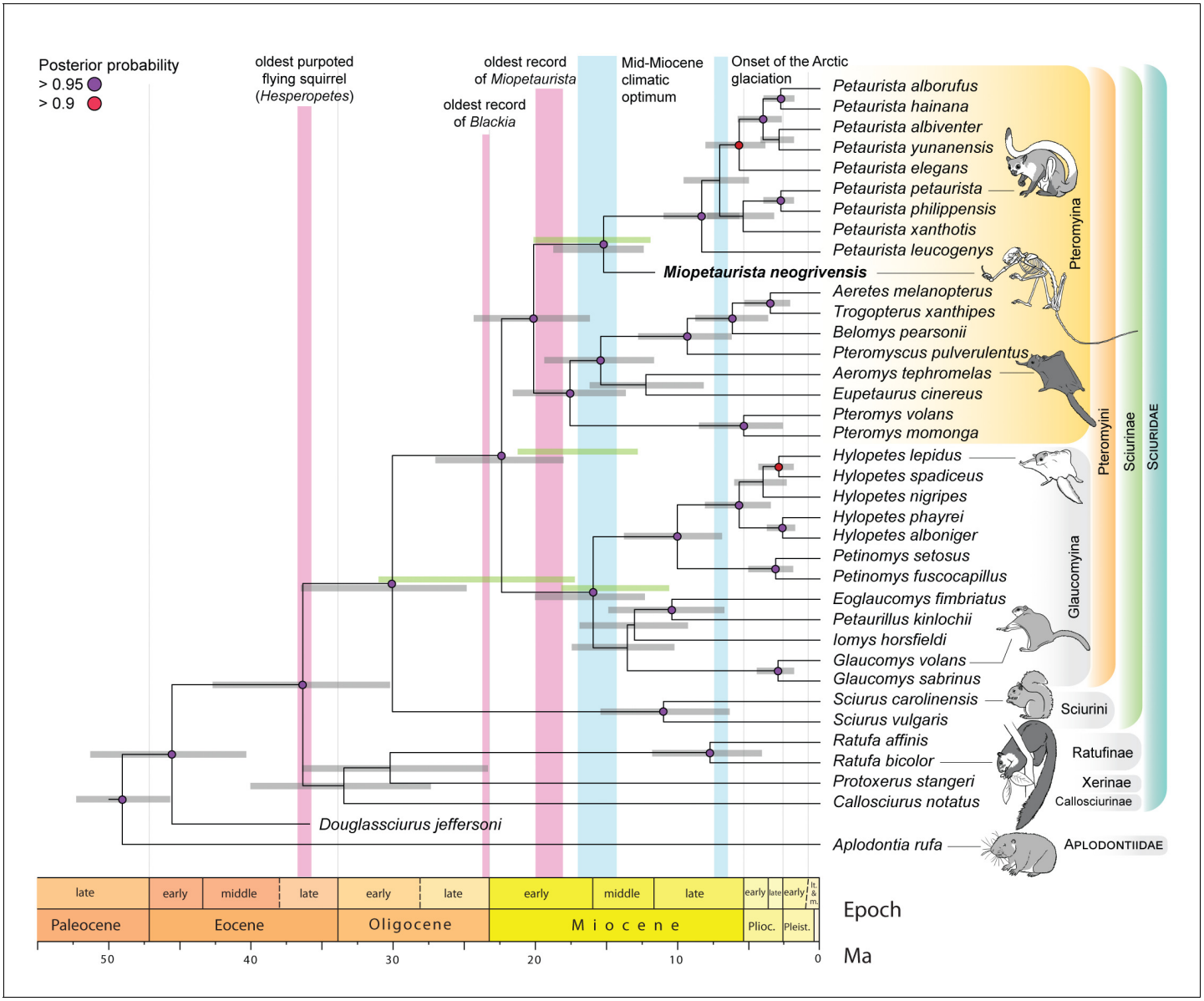

Figure 7. Flying squirrel phylogeny and node dating estimates based on a Bayesian total evidence analysis including *Miopetaurista neogrivensis*. The analysis is based on 38 taxa, 105 morphological characters and 3345 base pairs (see Materials and Methods and Appendix 1.1). Purple circles at the nodes indicate posterior probabilities higher than 0.95. Error bars (gray shading) at the nodes are 95% highest posterior density (HPD) intervals for divergence dates. For selected nodes, 95% HPD intervals derived from an independent node dating analysis using BEAST (***Figure 7—figure supplement 1***) are also shown as green bars. Note the position of *Miopetaurista neogrivensis* as sister taxon of extant *Petaurista*. The age of the oldest purported flying squirrels in the fossil record as well as that of the earliest representatives of the genera *Blackia* and *Miopetaurista* is indicated for comparison (see also ***Figure 8***). Two major global climatic events are also indicated. The morphological character list is given in Appendix 2. Genbank accession numbers for all the sequences used in phylogenetic analyses are given in ***Supplementary file 2*** and morphological character matrix is given in ***Supplementary file 3***.

DOI: https://doi.org/10.7554/eLife.39270.020

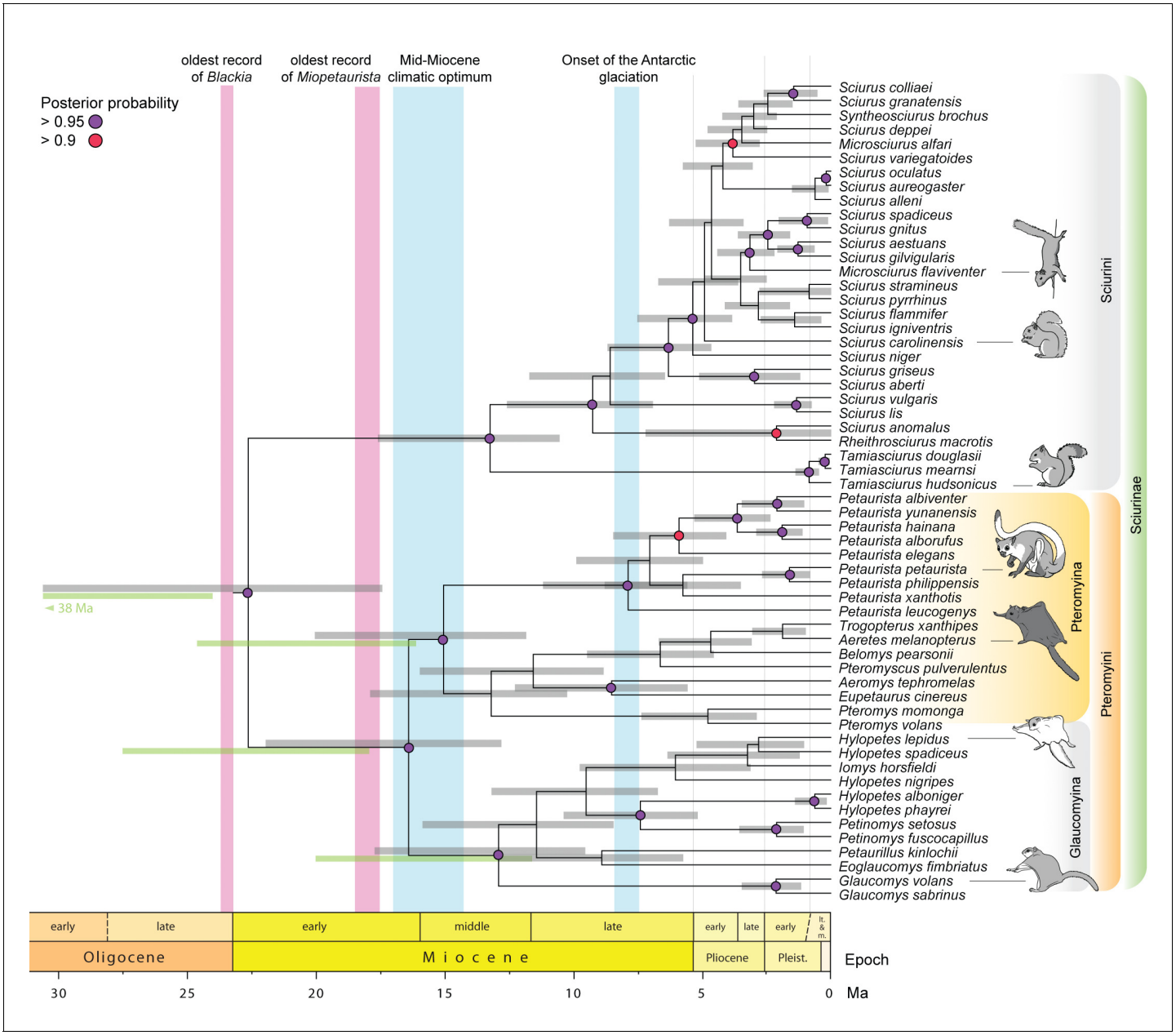

Figure 7—figure supplement 1. Sciurinae phylogeny and node dating estimates using BEAST. Based on 58 extant taxa and 3345 base pairs (see Materials and Methods and Appendix 1.2). The extinct *Miopetaurista neogrivensis* and *Douglassciurus jeffersoni* are used as calibration points. Purple and red circles at the nodes indicate posterior probabilities higher than 0.95 and 0.9, respectively. Error bars (grey shading) at the nodes are 95% highest posterior density (HPD) intervals for divergence dates. For selected nodes, 95% HPD intervals derived from an independent total evidence analysis (***Figure 7***) are also shown as blue bars. The age of the oldest purported flying squirrels in the fossil record as well as that of the earliest representatives of the genus *Miopetaurista* is indicated for comparison (see also ***Figure 8***). Two major global climatic events are also indicated. Fossils used in the calibration are given in ***Table 4*** (see also Appendix 1.2). Genbank accession numbers for all the sequences used in phylogenetic analyses are given in ***Supplementary file 2***.

DOI: https://doi.org/10.7554/eLife.39270.021

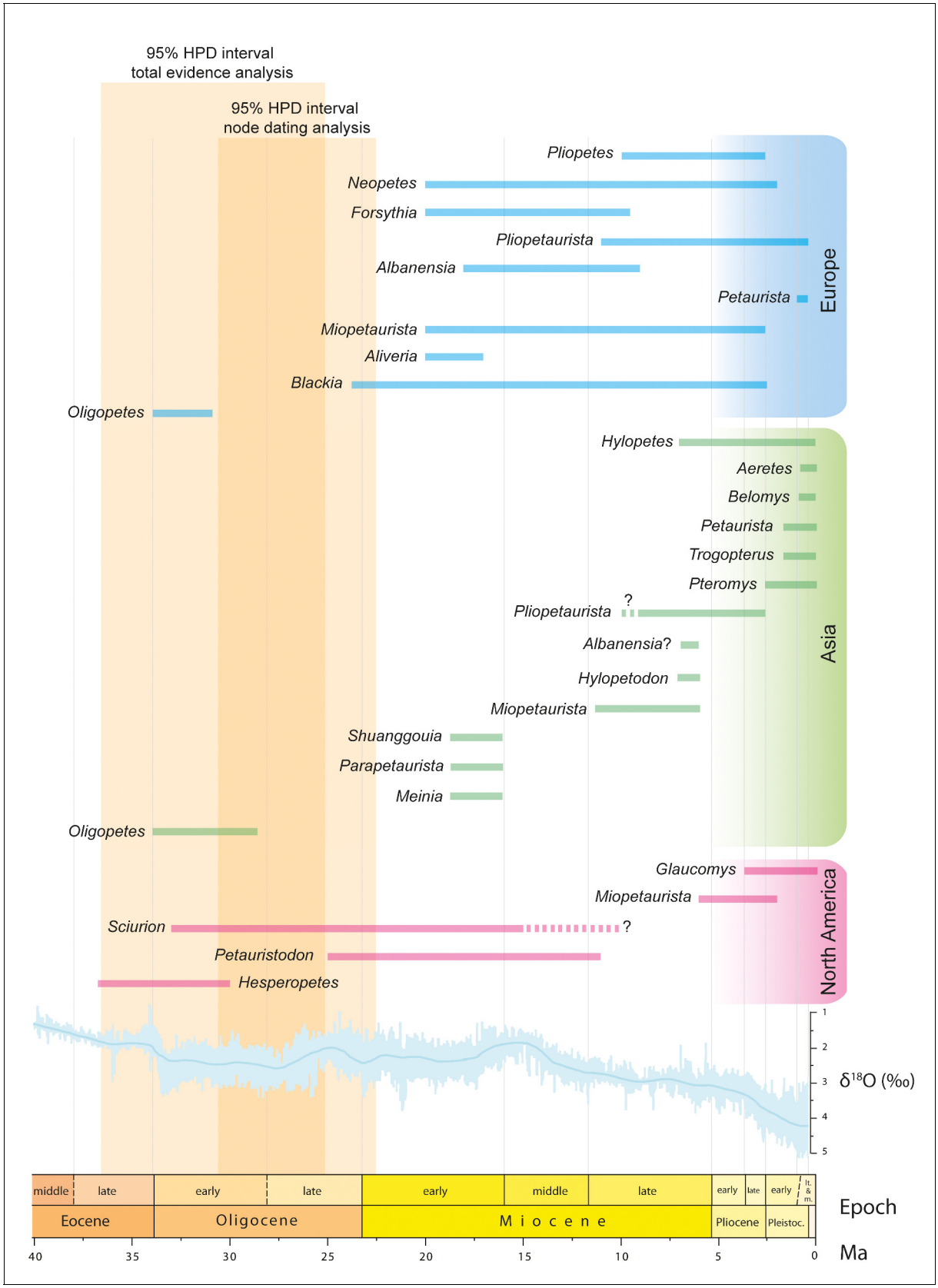

Figure 8. Fossil record of 'flying squirrels' and paleoclimatic data. Temporal ranges of purported flying squirrel genera in Europe, Asia and North America. The 95% highest posterior density (HPD) intervals for flying squirrel divergence as derived from total evidence and node dating analyses are

Figure 8 continued on next page

Figure 8 continued

indicated in orange shading (see ***Figure 7*** and ***Figure 7—figure supplement 1***). Darker shading indicates the time interval where both independently calculated estimates overlap, thus defining the most likely time interval for flying squirrel divergence. Global paleoclimatic data are taken from ***Zachos et al., 2001***.

DOI: https://doi.org/10.7554/eLife.39270.023

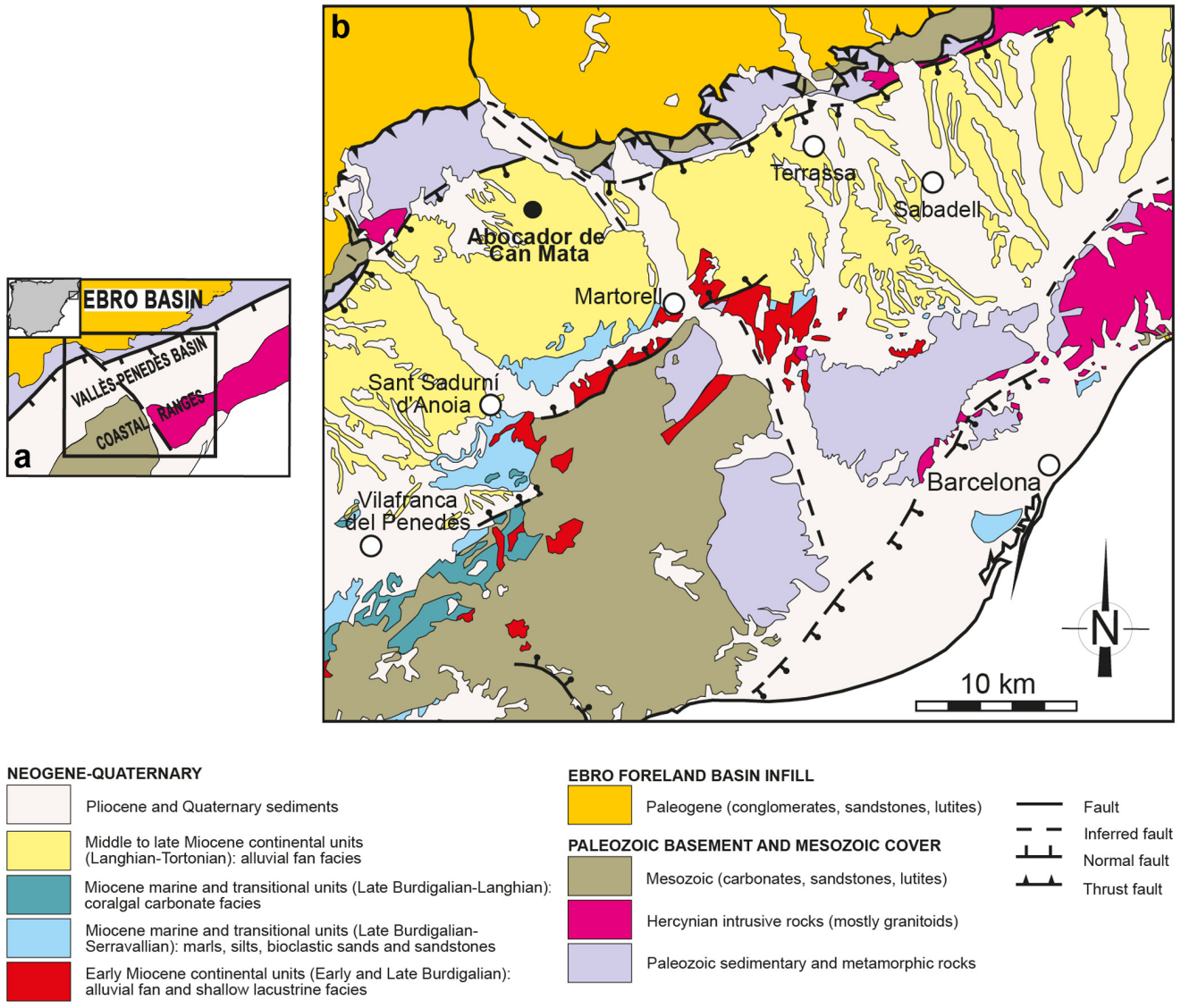

Figure 9. Geological map of the Vallès-Penedès Basin and situation of the fossil site. (**a**) Schematic geological map of the Vallès-Penedès Basin (Catalonia, Spain) showing the area enlarged in ***Figure 9b***. The inset shows its location within the Iberian Peninsula. (**b**) Situation of the Abocador de Can Mata series, located in distal alluvial fan facies of middle to late Miocene age. See ***Alba et al., 2017*** for further details on the stratigraphy and chronology of the Abocador de Can Mata series and main sites. Map modified from ***Casanovas-Vilar et al., 2016***.

DOI: https://doi.org/10.7554/eLife.39270.024